



Observations of root hair patterning in soils: Insights from synchrotron-based X-ray computed microtomography

Patrick Duddek · Andreas Papritz ·
Mutez Ali Ahmed · Goran Lovric ·
Andrea Carminati

Received: 5 October 2023 / Accepted: 21 February 2024 / Published online: 3 May 2024
© The Author(s) 2024

Abstract

Background And Aims Root hair emergence is affected by heterogeneities in water availability in the growth medium. Root hairs preferentially emerge into air, whereas their emergence into water is inhibited. Yet, these results were based either on destructive methods or on roots grown on an agar-air interface. Additionally, there is a lack of knowledge about the spatial distribution of root hairs as hairs elongate radially across the rhizosphere. Therefore, root hair growth in soils remains largely unexplored.

Methods Maize (*Zea Mays* L.) plants were grown in microcosms which were scanned with a synchrotron-based X-ray μ CT. The distribution of root hairs along

the root epidermis and radially across the rhizosphere (i.e. as function of distance from the root epidermis) was analysed using spatial point pattern analysis.

Results While hairs emerged randomly in air-filled pores, their emergence was inhibited where the root was in contact with the soil matrix. As hairs elongated radially into the soil, they were preferentially located in the close proximity of soil particles. In maize, we rarely observed root hairs penetrating into soil aggregates.

Conclusion We conclude that in maize, root hairs grow in air-filled pores at the root-soil interface, where the flow of nutrients and water is impeded. Across the rhizosphere, hairs establish contact to the soil by growing in the proximity to soil particles. The effect of hairs on uptake processes, plant anchorage and rhizosheath formation might be limited (in maize) as they hardly penetrate into soil aggregates.

Responsible Editor: Jiayin Pang.

Supplementary Information The online version contains supplementary material available at <https://doi.org/10.1007/s11104-024-06582-1>.

P. Duddek (✉) · A. Papritz · A. Carminati
Department of Environmental Systems Science, Physics
of Soils and Terrestrial Ecosystems, Institute of Terrestrial
Ecosystems, ETH Zürich, Universitätsstrasse 16, 8092
Zurich, Switzerland
e-mail: patrick.duddek@usys.ethz.ch

M.A. Ahmed
Chair of Root-Soil Interactions, TUM School of Life
Sciences, Technical University of Munich, D-85354
Freising, Germany

G. Lovric
Swiss Light Source, Paul Scherrer Institute, Forschungsstrasse
111, 5232 Villigen, Switzerland

Keywords Root hairs · Root plasticity · Cell fate · Rhizosphere

Introduction

In the pursuit of soil resources, root hairs, tubular protrusions of epidermal root cells, have been shown to be a beneficial root trait. By substantially increasing the contact area between roots and soil and thus the volume of soil affected by roots, they facilitate the uptake of nutrients, particularly those with limited mobility in

soil systems (e.g. phosphorus, Bates and Lynch 1996, Haling et al. 2013, Miguel et al. 2015, Misra et al. 1988, Singh Gahoonia et al. 1997, Zhu et al. 2010). In addition, when the root-soil contact is loose and the soil is dry, they facilitate root water uptake by bridging low conductivity air gaps at the root surface (Robbins and Dinneny 2015). Thereby, they attenuate gradients in soil matric potential at the root-soil interface (Carminati et al. 2017, Duddek et al. 2023, Marin et al. 2021). However, at very negative soil matric potentials the effect of hairs on uptake processes may be hindered by hair dehydration and shrinkage (Duddek et al. 2023). Root hairs have also been shown to favour plant anchorage (Bengough et al. 2016), rhizosheath formation (Burak et al. 2021) and carbon exudation (Holz et al. 2018). Their impact on these processes is influenced by their contact with the soil matrix and hence by their spatial emergence along the root epidermis and how they elongate into the soil.

Root hair development is regulated by genetic factors, plant hormones and environmental controls. Bibikova and Gilroy (2002), Dolan and Costa (2001), Müller and Schmidt (2004), Salazar-Henao et al. (2016), Zhang et al. (2023) give comprehensive reviews of the mechanisms underlying the development of root hairs. Epidermal cells in most vascular plants are classified in root hair cells (trichoblasts) and non-root hair cells (atrichoblasts). The spatial arrangement of these cell types has been investigated for a variety of plant species. Thereby, three distinct root hair emergence patterns have been identified. In the type III pattern (e.g. in *Arabidopsis*), trichoblasts are located at the junction of two underlying cortical cells resulting in root hair cell files, which are surrounded by cell files of atrichoblasts (Bünning 1951, Dolan et al. 1994). In the type II pattern (e.g. rice), cell fate depends on asymmetric epidermis cell division, with the smaller cells forming trichoblasts and the larger cells forming atrichoblasts (Clowes 2000, Pemberton et al. 2001). In the type I pattern (e.g. maize), root hairs potentially form from any epidermal root cell regardless of their position in relation to cortical cells or cell size, which is expected to result in a highly plastic emergence pattern.

Nevertheless, root hair plasticity in response to various environmental signals was found to be independent of pattern type (Clowes 2000, Cormack 1944, 1947). For example, phosphorus availability has been

shown to have a fundamental effect on root anatomy, causing changes in root hair density (Ma et al. 2001). The authors found that root hair density of *Arabidopsis* increased massively in phosphorus-deficient growth media. Additionally, Zhu et al. (2005) observed that maize root hairs responded to phosphorus deficiency by increasing their length. Foehse and Jungk (1983) obtained a similar result, but also noted that root hair length and density were affected by phosphorus content in the plant rather than by the phosphorus content at the root surface. It is worth noting that these results originate from roots grown in nutrient solution. They contradict a field study based on 8 weeks old maize roots, where no significant effect of phosphorus on root hairs was found (Anderson et al. 1987). On the other hand, Mackay and Barber (1985) demonstrated by a pot experiment that root hair density and growth was more affected by soil moisture than phosphorus availability. The authors also studied the response of root hair growth to soil drying and wetting cycles (Mackay and Barber 1987). In agreement with their former experiment, they found that root hair growth was promoted by dry soil and reduced by wet soil conditions. When analyzing roots and root hairs in field cores, White and Kirkegaard (2010) found that root hair emergence patterns differed between roots growing through pores and cracks. Root hair density was negatively correlated with root-soil contact: root hair density dropped exponentially with increasing root-soil contact. It was hypothesised that roots growing through macropores relied on root hairs providing root-soil contact. The observations reviewed above suggest that the increase in root hairs might be a response to water availability. Indeed, it has been shown that root hairs have evolved mechanisms to sense and respond to the distribution of water. Bao et al. (2014) demonstrated that root hair emergence is controlled by heterogeneity in water availability. Roots of *Arabidopsis*, maize and rice were grown at the surface of a vertically placed agar medium and the authors monitored the development of lateral roots and root hairs. They observed that lateral roots predominantly formed on the agar contact side of the root, a mechanism termed hydropatterning, which is regulated by an auxin gradient across the root radius in response to water availability (Giehl and von Wirén 2018, Orosa-Puente et al. 2018). Conversely, root hairs preferentially emerged at the air side of their experimental setup. Yet,

the mechanism of root hair patterning remains unclear, and Bao et al. (2014) found that root hair initiation on the agar contact side could be rescued by a treatment with abscisic acid (ABA) and the ethylene precursor 1-aminocyclopropane-1-carboxylic acid (ACC). Scanning soil-grown root systems using an X-ray CT, Bao et al. (2014) showed that hydropatterning of lateral roots also occurred in physiologically relevant conditions. However, the spatial resolution of their CT scans (actual pixel size: 22 μm) was not sufficient to study the patterning of root hairs.

So far, root hair emergence patterns in soils have not been investigated non-destructively and *in situ*. Furthermore, information on the spatial distribution of root hairs as function of the distance from the root epidermis is lacking. This knowledge is of particular interest to better understand the effect of root hairs on nutrient and water uptake, plant anchorage, rhizosheath formation and the interaction between roots and microorganisms. Especially for nutrient and water uptake, mathematical models are based on the assumption of uniformly distributed root hairs within a homogeneous soil (Itoh and Barber 1983, Leitner et al. 2010, Segal et al. 2008, Zygalkis et al. 2011). Given the patterning of root hairs (Bao et al. 2014) and the distinct hydraulic properties of the rhizosphere compared to the bulk soil (Carminati et al. 2010, Gregory 2006, Hinsinger et al. 2009, Lavelle 2002, Watt et al. 2006), this might not be a safe assumption. So far only image-based nutrient and water uptake models inherently include this spatial complexity throughout the rhizosphere. However, these models are computationally highly expensive, and their predictive power on large scales is limited.

Therefore, the objective of this study was to determine, non-destructively and *in situ*, a general pattern of root hair emergence and growth. In particular, we tested whether the distribution of maize root hairs both along the root epidermis and as a function of distance from the root epidermis was spatially random or followed a non-random pattern. This was achieved by collecting high-resolution image data of maize (*Zea Mays* L.) roots and root hairs using synchrotron-based X-ray computed microtomography (CT). After image processing, we conducted a spatial point pattern analysis to analyse the spatial distribution of root hairs along the root epidermis and within the rhizosphere. Spatial point pattern analysis is a powerful geo-statistical

method, that has been used extensively in plant ecology to unravel pattern-process relationships and biotic interactions (Ben-Said 2021).

In the present work, we applied it to evaluate the following hypotheses:

1) We hypothesized that root hairs preferentially emerge (a) into the air-filled pore space and (b) in the close vicinity of contact surfaces between roots and soil particles.

2) We hypothesized that the distal segments of root hairs are preferentially located in the close vicinity of soil particles or aggregates.

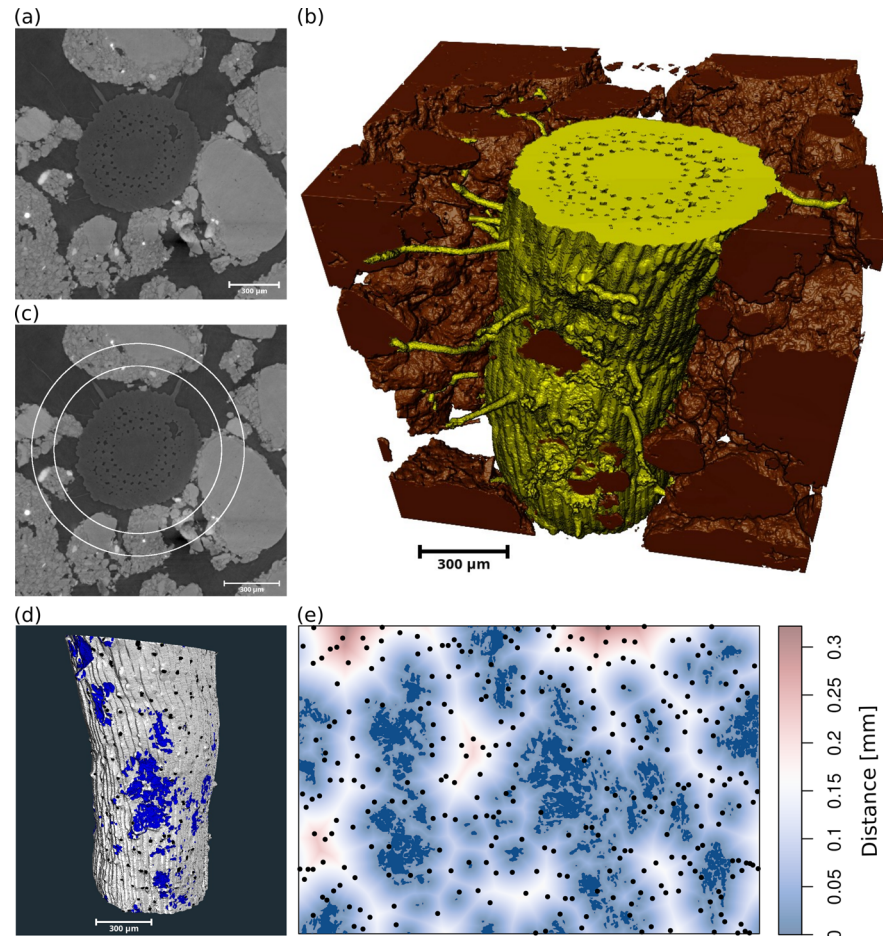
The rationale for (1a) was based on the observed root hair patterns of Bao et al. (2014) and the results of White and Kirkegaard (2010). Hypothesis (1b) was based on the assumption that root hair emergence in the close proximity to soil particles may facilitate hair-soil contact establishment compared to randomly emerging hairs. The rationale for 2) was that root hairs attached to soil aggregates were able to extract soil resources even though soil macropores had been drained. Such hairs would also improve plant anchorage and rhizosheath formation.

Materials and methods

We grew maize seedlings in microcosms and scanned plastic cylinders containing a loamy soil and maize roots in a synchrotron X-ray μCT . After image segmentation, we extracted root hair emergence points, the root epidermis and the root-soil contact area. Based on the assumption of cylindrical root segments, we projected the data from 3D to 2D-surfaces and conducted a replicated spatial point pattern analysis, which gave statistical insights into spatial patterns of root hairs along the root epidermis.

We then replaced the root segments in the images with cylinders of radius ‘mean root radius plus 1) half of the mean root hair length and 2) the mean root hair length’ (Fig. 1c). We will refer to these cylinders as ‘rhizosphere cylinders’ in the remainder of the text. This definition is functional to define the 2D surface for the analysis of root hair distribution. We repeated the replicated spatial point pattern analysis on the rhizosphere cylinders to assess the distribution of root hairs radially across the rhizosphere (i.e. as a function of distance from the root epidermis into the soil).

Fig. 1 Overview of the image processing pipeline. (a) Reconstructed 2D slice of the raw data showing a root with root hairs (medium grey), air-filled pore space (black) and soil particles (light grey, scale bar = 300 μm). (b) 3D rendering of the segmented data showing a root segment with turgid root hairs (yellow) and the soil matrix (brown, scale bar = 300 μm). (c) Same 2D slice as in (a) with two white circles indicating rhizosphere cylinders (distances to the epidermis: inner circle: 122.75 μm , outer circle: 245.5 μm , scale bar = 300 μm). (d) 3D rendered root segment (white) showing root-soil contact surface (blue) and root hair emergence points (black, scale bar = 300 μm). (e) 2D plot of the unwrapped root epidermis (from (d)) as distance map (dark blue: root-soil contact) and the root hair emergence points (black)



Plant growth

Maize (*Zea Mays* L., B73 wild-type) plants were grown in 3D-printed seedling holders. Each seedling holder was connected to seven 1.3 ml plastic cylinders (80 mm length, 4.5 mm diameter) and the setups were filled with a fertilized loamy soil at a dry bulk density of 1.2 g cm⁻³. In total, 13 plants were grown for 14 days under controlled conditions in a climate chamber at a relative air humidity of 65% and a temperature of 22°C during day (12h) and 18°C during night (12h). Volumetric water content of the samples was checked daily and readjusted to 0.22 cm³ cm⁻³. This translated into a soil matric potential of approx. -0.03 MPa (estimated based on the water retention curve of the used soil texture, Vetterlein et al. 2021). As reported by Duddek et al. (2023) the macropores in the used soil texture were drained at this matric potential.

Imaging and image processing

As water and roots have similar X-ray attenuation, the respective grey scale values overlap in the image data, which makes it difficult to distinguish between roots and water-filled pore space. To increase the contrast between roots and macropores, we stopped watering the plants two days before imaging, resulting in drained macropores at the time of scanning. Plants were transported alive to the X02DA TOMCAT beamline of the Swiss Light Source synchrotron (Paul Scherrer Institute, Villigen, Switzerland). Shortly before scanning individual plastic cylinders, roots were cut with a razor blade and the plastic cylinders were disconnected and sealed with parafilm. In total 48 scans of 16 cylinders and 8 individual plants were performed. The present study is based on four scans of three cylinders and three individual plants (four technical replicates,

three biological replicates), published in Duddek et al. (2022). Regarding data selection, only samples containing turgid roots could be used in this study, as dehydrating roots shrink and recede so that the position of root hair emergence points in relation to the soil matrix changes. As turgid root hairs indicate that also the corresponding roots are fully turgid (Duddek et al. 2022), we only considered those samples that contained a considerable amount of turgid root hairs.

The actual voxel size of the images (Fig. 1(a)) was $0.65 \times 0.65 \times 0.65 \mu\text{m}^3$ which enabled us to sharply resolve root hairs. A comprehensive description of the beam and detector setup is available in Duddek et al. (2022, supporting information).

Each reconstructed dataset consisted of 2160 images per stack and exhibited a physical size of $3.05 \text{ mm} \times 2.28 \text{ mm} \times 1.40 \text{ mm}$. The image data were processed in Avizo Thermo Fisher Scientific (2020). After a conversion from 16bit to 8bit, an Unsharp Masking filter (2D) was applied to account for the Paganin low-pass filter occurring prior to the CT reconstruction. The data was segmented by applying a marker-based watershed transformation which resulted in a label field consisting of soil matrix (including water-filled micropores), air-filled pore space and roots including turgid root hairs (Fig. 1(b)). Subsequently, the root and root hair domains were separated by applying a morphological opening and the root hairs were added to the label field as an independent label. As we could not segment dehydrated root hairs using the aforementioned approach, root hair emergence points were labelled manually and added to an independent label in the label field. The root volume was determined by applying a label analysis and both the mean root radius and the mean root circumference were calculated based on the root volume, the length of the root segment and the assumption of a cylindrical root segment. If a root segment grew along the plastic cylinder wall, the part facing the cylinder wall typically did not contain any root hairs and was excluded from further analysis. This applied to two of four samples (samples 01 and 03).

Based on the label field consisting of the materials 1) soil matrix, 2) air-filled pore space, 3) root, 4) root hairs and 5) root hair emergence points, a surface mesh was generated in Avizo. Finally, the root epidermis, root hair emergence points and the interface between root epidermis and soil particles (root-soil contact) were exported as individual triangular meshes in the stl-format (Fig. 1(d)).

Unwrapping

The exported meshes were unwrapped, meaning that the surface meshes generated in 3D were projected onto a 2D-surface (UV mapping). This was achieved using the ‘Cylinder Projection’ tool in Blender (Blender Online Community 2002). Thereby, the aspect ratio of the meshes was maintained and the basic assumption of this transformation was that the root segments were cylindrical. Finally, we exported the unwrapped data in the stl-format (Fig. 1(e)).

The unwrapped meshes of 1) the root-soil contact, 2) the root hair emergence points and 3) the root epidermis were imported in Cloud Compare (Girardeau-Montaut 2002) and scaled according to the previously calculated mean root circumference and length of the corresponding root segment. By computing the concave hull (Cross Section tool in CloudCompare), the contours of the root epidermis were extracted as polylines and exported as svg-files. The contours of the root hair emergence points were generated as well and the centre of each emergence point was calculated and exported in the csv-format. The latter resulted in a set of root hair emergence points in Cartesian coordinates.

The stl-file containing the unwrapped root-soil contact was imported in Avizo and converted to a binary image. If the root was not growing along the plastic cylinder wall, we mirrored the image on the right and left boundary. This way, we created periodic boundaries in the binary image, meaning that we took the cylindrical shape of the root into account. If the root was growing along the cylinder wall, we did not mirror the data, but instead removed the part facing the wall (as described above). We then applied a Euclidean distance transform, cropped the resulting distance map to its original size (in the case of periodic boundaries, Fig. S1), and exported it as a tiff file. This distance map included the Euclidean distance from each pixel of the root epidermis to the nearest root-soil contact (Fig. 1(e)).

To test hypothesis 2), we assessed whether root hairs grew uniformly across the rhizosphere or whether their position depended on the distance to soil particles. To this end, we constructed the so-called rhizosphere cylinders: Based on the label field containing the root, we calculated the centre of mass of the root domain in each slice of the image stack. We then placed a circle into each slice, the origin of which corresponded to the root centre of mass, and the radius of the circle was

equal to the mean root radius (constant for the entire stack of slices and determined as described above) plus 1) one half of the mean hair length (122.75 μm) or 2) plus the mean hair length (245.5 μm) reported in Duddek et al. (2022) (Fig. 1 (c)). After replacing the root domain in the label field by the generated cylinders, the intersections of the rhizosphere cylinders with root hairs (we will refer to them as ‘intersection points’) were added manually to the label field. Repeating the aforementioned procedure, we subsequently generated triangle meshes of the rhizosphere cylinders, the intersection points and the interface between the rhizosphere cylinders and soil particles. We then repeated the previously described approach to unwrap the data and to generate Euclidean distance maps representing the distance from each pixel across the rhizosphere cylinders to the closest rhizosphere cylinder - soil matrix contact. The 2D-plots of the unwrapped root epidermis and the two unwrapped rhizosphere cylinders, including the generated distance maps and emergence or intersection points, respectively are available for all samples in Fig. S2 - S5.

Spatial point pattern analysis

The spatial point pattern analysis was conducted using the ‘spatstat’ library, (Baddeley et al. 2015, version 3.0-3) in R (RCore Team 2022, version 4.2.1) with the front-end RStudio (RStudio Team 2002, 2022.02.3). To study the distribution of root hair emergence points on the epidermis, the envelopes of the root epidermis, the distance maps of epidermis-soil contacts and the coordinates of root hair emergence points were imported to R. To study the distribution of root hairs radially across the rhizosphere, the envelopes of the rhizosphere cylinders, the distance maps of rhizosphere cylinder-soil contacts and the coordinates of root hair intersection points were imported to R. To conform to the jargon of spatial point pattern analysis, we will refer to both root hair emergence points and root hair intersection points as ‘events’ in the remainder of the text.

The key assumption of the study was that root hairs were distributed over the epidermis and the rhizosphere cylinders according to a Poisson process. The assumption behind the replicated point pattern analysis is that the four samples are independent replicates of the same point process and that they are comparable to each other (Baddeley et al. 2015).

Homogeneous Poisson point process

The homogeneous Poisson point process model was utilized as null-model to test whether the intensity, i.e. the spatial density of root hairs on the epidermis and within the rhizosphere was spatially constant or depended on the distance to the soil particles. A homogeneous Poisson point process \mathbf{X} is characterized by two fundamental properties (Baddeley et al. 2015, Diggle 2013, Illian et al. 2008).

1. The number $n(\mathbf{X} \cap W)$ of events falling in any region W exhibits a Poisson distribution with mean $\lambda \cdot |W|$. Here, λ represents the constant intensity (number of events per mm^2 of region W) and $|W|$ the surface area of region W .
2. The numbers of events n in k disjoint regions B_1, B_2, \dots, B_k are independent random variables for arbitrary k .

Points resulting from a homogeneous Poisson process are randomly distributed in space. The homogeneous Poisson process is commonly considered as the archetype model for ‘complete spatial randomness’ (CSR).

Inhomogeneous Poisson process

Releasing the assumption of a constant in favour of a spatially varying intensity in item 1. above leads to the definition of the inhomogeneous Poisson process (Baddeley et al. 2015, Diggle 2013, Illian et al. 2008). More precisely, the spatially constant intensity λ is replaced by a non-constant intensity function $\lambda(u)$, depending on the spatial location u . The number of events in any subregion B follows a Poisson distribution with mean $\int_B \lambda(u) du$.

The independence property (see 2. above) is also valid for an inhomogeneous Poisson point process. Comprehensive summaries of further general properties of both homogeneous and inhomogeneous Poisson point processes are available in Baddeley et al. (2015), Diggle (2013), Illian et al. (2008), Wiegand and Moloney (2013).

Testing spatial correlation

To analyse the spatial correlation of the point patterns (inter-point dependence), summary statistics based on

the spacing between events were calculated. In general, a test for inter-point dependence has three possible outcomes: 1) The events are clustered, meaning that a typical event of the pattern has more neighbours than expected by CSR; 2) The point process is regular, meaning that a typical event of the pattern has less neighbours than expected by CSR; or 3) The events are distributed according to CSR.

Nearest neighbour distance distribution function $G(r)$ and empty space function $F(r)$

To reveal information on the spatial arrangement of the events, both the nearest neighbour distance distribution function $G(r)$ and the empty space function $F(r)$ were calculated. These cumulative distribution functions (CDFs) are particularly suitable to study local interactions of events (Wiegand and Moloney 2013).

In a point process \mathbf{X} , the G -function characterises the shortest distance from an arbitrary event x_i to the pattern $\mathbf{X} \setminus x_i$. Thus, the G function estimates the probability of another event existing within a distance r of an arbitrary event x_i .

In contrast, the empty space function $F(r)$ calculates the distance from an arbitrary reference location $u \in \mathbb{R}^2$ (which does not coincide with an event) to the closest event of the process. Hence, the F -function estimates the probability of finding an event in a radial distance r from an arbitrary reference location u .

Note that for a completely random pattern (homogeneous Poisson Point process), the distributions of both the nearest neighbour distances and of the empty space distances are equal, while they differ for general point processes.

Comprehensive descriptions including the mathematical foundation of the G - and F -functions and the DCLF-test are available in Baddeley et al. (2015), Diggle (2013), Illian et al. (2008), Wiegand and Moloney (2013).

The G - and F -functions (null hypothesis: CSR of the four samples) were estimated using the ‘Gest’ and ‘Fest’ functions of the ‘spatstat’ library. The option ‘best’ was selected for edge correction. Subsequently, the resulting G - and F functions were pooled over the four samples using the ‘pool’ function of spatstat.

Additionally to the computation of the G - and F - functions, which allowed a visual assessment of whether or not the point patterns resulted from CSR, we followed the recommendation of Diggle (2013) and conducted a Monte Carlo test with the integrated squared deviation of the G - and F - functions from

their theoretical values under CSR as a test statistic. This hypothesis test is termed as the ‘Diggle-Cressie-Loosmore-Ford (DCLF) test’ and was applied calling the ‘dclf.test’ function in spatstat. The resulting sample-wise p-values of the DCLF-tests were pooled by calculating their harmonic mean using the ‘hmp.stat’ function of the ‘harmonicmean’ package (Wilson 2019).

A methodological limitation of our analysis is related to the fact that the non-negligible, finite spatial extent of an emergence or an intersection point of a root hair was neglected. Its position was approximated merely by a point of infinitesimal size (optimally located in the centre of a emergence or intersection point). But the spatial extent of the root hair cells on the epidermis and root hair extent in more distal parts of the hairs actually provide a physical lower bound as to how close two recorded events can get to each other and how close they can get to soil particles. This means that along the epidermis, two root hairs cannot get closer to each other than the diameter of an epidermal cell (0.0215 mm, Steudle et al. 1987), and they cannot get closer to soil particles than 0.01075 mm. Across the rhizosphere, two turgid root hairs cannot be detected closer than 0.01788 mm (mean root hair diameter) and they cannot get closer to soil particles than 0.00894 mm (mean root hair radius). Nevertheless, the negligence of the finite size of the root hairs and root hair cells can be justified by the fact that both the root epidermal cell diameter and the root hair diameter are at least two orders of magnitude smaller than the edge length of the observation windows (Baddeley et al. 2015).

Testing the dependence of the intensity on the distance to soil particles

To test whether the distribution of events on the root epidermis and throughout the rhizosphere depended on the distance to soil particles, we conducted formal tests of dependence on a covariate. For all tests, the null hypothesis was that the intensity was homogeneous, the alternative hypothesis was that the intensity was inhomogeneous, and the significance level was selected as $\alpha = 0.05$.

To test the homogeneity for the root epidermis, the observation windows were divided into two tiles, and a quadrat counting test of homogeneity was applied. To address the aforementioned neglect of the phys-

ical root epidermal cell diameter, the first tile ('Root - soil contact', Fig. 3) covered the distance interval $[0, 0.0215]$ mm, which means that all root hairs that emerged at the root-soil contact were included in this tile. We used the mean epidermal cell diameter (0.0215 mm) instead of the corresponding radius as the upper boundary of the interval, because the locations of root hair emergence points had been marked manually, which may have introduced some spatial errors in the recorded positions. Therefore, using the diameter of the epidermal cells rather than their radius as the upper limit for the first tile resulted in a more conservative analysis.

The second tile ('Pore space', Fig. 3) covered the distances from 0.0215 mm to the maximum distance in the observation windows. This allowed us to test whether root hairs preferentially emerged into air-filled pore space or into partially water-saturated soil aggregates (hypothesis 1a). We performed sample-wise chi-square tests of uniformity, which relate the event counts within each tile to the number of events predicted by the model assuming homogeneous intensity. The sample-wise results were pooled by calling the 'pool' function. Due to their better statistical performance, we additionally conducted sample-wise Berman's Z_2 tests (Berman 1986) by applying the 'berman.test' function in spatstat. The results were pooled by calculating their harmonic mean as described above.

To test the homogeneity of the distribution of events on the rhizosphere cylinders, the observation windows were divided into three tiles. The first tile ('rhizosphere cylinder - soil contact', Fig. 6) covered the distance interval $[0, 0.01788]$ mm, which corresponds to the mean diameter of the root hairs (Duddek et al. 2022). The intervals for the second and third tiles ('pore space close to soil' and 'pore space distant from soil', Fig. 6) were selected such that the remaining part of the observation window was split into two parts of equal area. On these three tiles, we performed pair-wise chi-square tests and again pooled the results. Furthermore, we accounted for multiple testing by a Bonferroni correction (Neyman and Pearson 1928). This approach allowed us to study whether root hairs were preferentially located in certain distances from soil particles on the rhizosphere cylinders (hypothesis 2).

We further performed tests that take the exact values of the covariate at each event into account. The tests compare the cumulative distribution function (CDF) of

the covariate at the events with the spatial CDF of the covariate at all spatial locations within the observation window. For a point process with homogeneous intensity the two CDFs should be (approximately) the same.

To test this, we fitted a Poisson point process model to the hyperframe of the point patterns of all samples using the mppm function (spatstat) before performing a goodness of fit test based on the Kolmogorov-Smirnov statistic (Kolmogorov 1933) by calling the function 'cdf.test' in spatstat with the argument 'test = ks'. The model is based on the assumption that all point patterns are independent replicates of the same homogeneous Poisson process with variable intensity. Additionally, we conducted sample-wise Berman's Z_2 tests and pooled the results as described above.

Non-Parametric estimation of the intensity of the point process

To complement the analyses we estimated the dependence of the intensity on the distance to soil particles non-parametrically. To this end, one assumes that the intensity $\lambda(u)$ at any spatial location u within the observation window W can be expressed as a function of the covariate $Z(u)$:

$$\lambda(u) = \rho(Z(u)), \quad (1)$$

where ρ is the function to be estimated. This non-parametric estimation of $\rho(Z(u))$ was done by the 'rhat' function of the spatstat library. It relates the probability density of covariate values at all events within the observation window to the probability density of covariate values at random locations throughout the observation window. As kernel estimator, the 'reweighting' estimator was selected (Baddeley et al. 2012). The smoothing bandwidth was calculated by the 'density' function of the 'stats' package (Rodríguez-Álvarez et al. 2017, version 4.2.1) and multiplied by a factor of 2 in order to reduce oscillations in the results.

Discriminatory power of a covariate

To assess the strength of the dependence of the intensity of the point pattern on the covariate, the receiver operating characteristics (ROC) were generated. The ROC plot represents a probability-probability plot of CDF

values of the covariate at the events plotted vs. the spatial CDF at all locations. For a covariate exhibiting high discriminatory power, the ROC curve lies considerably above or below the 1:1 line. For a more quantitative assessment of the discriminatory power of a covariate, we calculated the area under the ROC curve (AUC). It's value ranges in the interval [0, 1]. Values close to 0 and 1 indicate strong discrimination, while a value of 0.5 indicates no discriminatory power (Baddeley et al. 2015). The results of the individual ROC-curves were pooled using the ‘pool’ function in spatstat. The corresponding AUC indices were evaluated by calculating

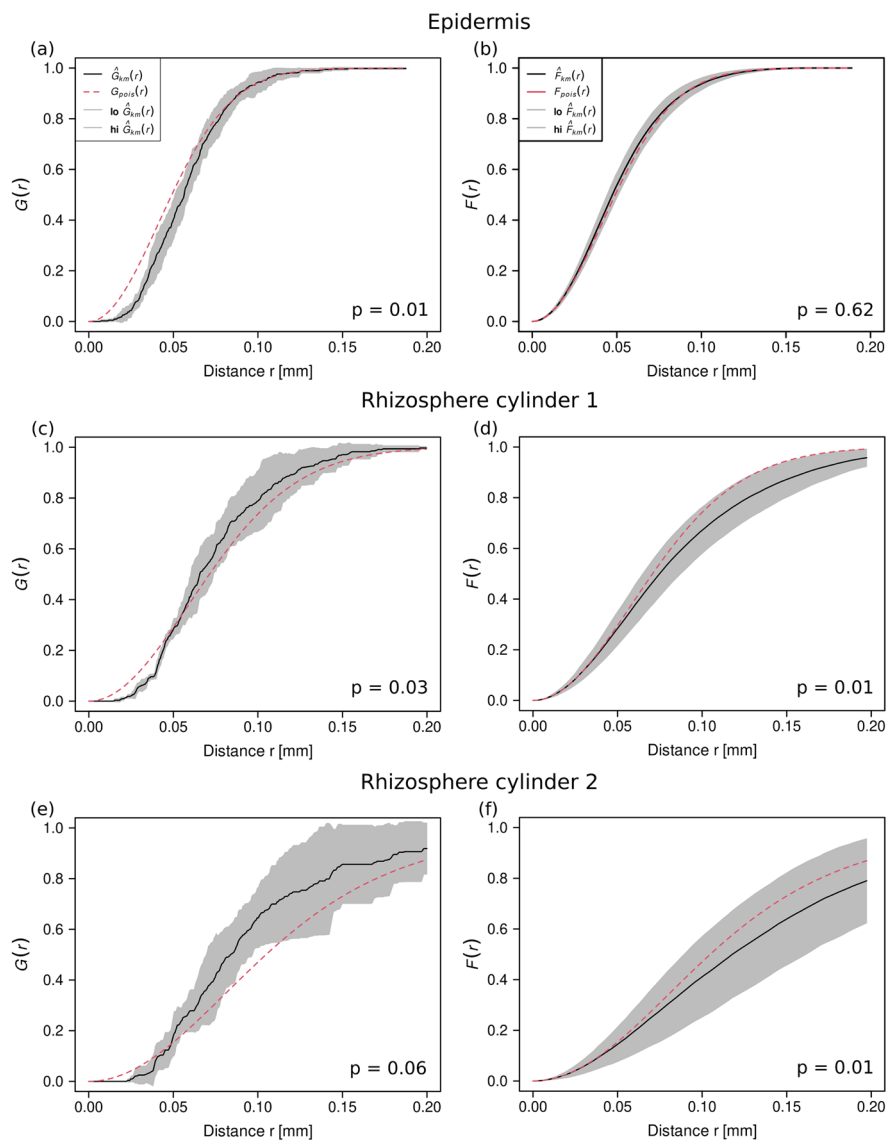
the arithmetic mean and the standard deviation of the individual AUC indices.

Results

Inter-point dependence on the root epidermis

At the epidermis, the four root sections analysed contained a total of 928 events with an average intensity of 90 ± 14 events/mm². Up to a distance of 0.06 mm, the pooled nearest neighbour distance distribution function

Fig. 2 Summary statistics for analysing the spatial correlation of root hair emergence and intersection points. (a), (c), (e): Pooled nearest neighbour distance distribution function $G(r)$ for point patterns along the root epidermis, rhizosphere cylinder 1 and rhizosphere cylinder 2. (b), (d), (f): Pooled empty space function $F(r)$ for point patterns on the root epidermis, rhizosphere cylinder 1 and rhizosphere cylinder 2. The $\hat{G}_{km}(r)$ and $\hat{F}_{km}(r)$ functions represent the spatial Kaplan-Meier estimates (Baddeley and Gill 1997) of the $G(r)$ - and $F(r)$ -functions, respectively. $G_{pois}(r)$ and $F_{pois}(r)$ represent the theoretical $G(r)$ - and $F(r)$ -functions for a stationary Poisson process of equal estimated intensity. The shaded areas represent the pointwise 95% confidence intervals of the $G(r)$ - and $F(r)$ -functions in between the lower (*lo*) and upper (*hi*) simulation envelopes. The presented p-values resulted from the pooled DCLF-tests



($G(r)$) deviated from CSR indicating a regular pattern (Fig. 2(a)). For distances > 0.06 mm, the G -function followed CSR. In contrast, the pooled empty space function ($F(r)$) did not significantly deviate from CSR (Fig. 2(b)). The results of both functions are supported by the presented pooled DCLF values (Fig. 2 (a) & (b)). The deviation of the G -function from CSR justified to further explore the effect of the covariate ‘distance to soil particles’ on the root hair emergence pattern.

Inhomogeneous intensity of root hair emergence on the root epidermis

The quadrat counting results on the root epidermis (Fig. 3) show a significantly ($p = 6.91 \cdot 10^{-8}$) reduced intensity of events at the root-soil contact. The results of the sample-wise chi-square tests (Table S1 and Fig. S9) were significant for three of four samples. These results suggested to reject the null hypothesis of a homogeneous intensity. While root hair emergence was inhibited at root-soil contact, hairs preferentially emerged into air-filled macropores.

Similarly, both the pooled Kolmogorov-Smirnov test ($p < 2.2 \cdot 10^{-16}$) and the pooled Berman Z2 test ($p = 3.5 \cdot 10^{-6}$) were significant, also indicating the rejection of the null hypothesis (CSR). The

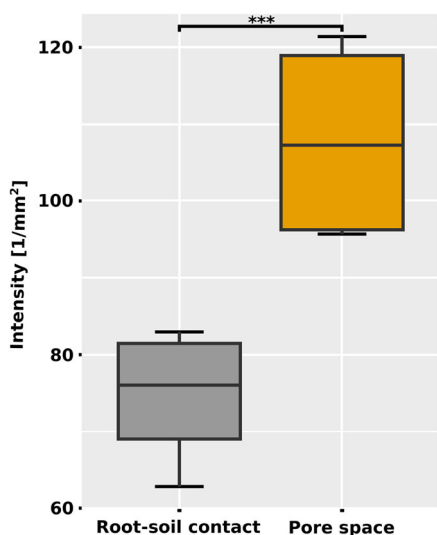


Fig. 3 Intensity of root hair emergence points on the epidermis. Pooled quadrat counting results for testing the dependence of the root hair distribution along the root epidermis on the covariate ‘distance to soil particles’ (***) $p < 0.001$)

sample-wise results of the analysis are presented in Table S2 and Fig. S12.

Visual inspection of the sample-wise results in Fig. S12 revealed that the CDFs of the covariate at the reported events were horizontally offset by about 0.01 mm compared to the spatial CDFs at all locations within the observation windows (under the assumption of CSR; dashed red line). This suggested that the rejection of the null-hypothesis (CSR) was caused by the inhibition at root-soil contact. To test this (hypothesis 1b), the distance interval $[0, 0.0215]$ mm to soil particles and the corresponding events were excluded before generating the CDFs and applying both the pooled Kolmogorov-Smirnov test and the pooled Berman Z2 test. The results ($p = 0.27$ and $p = 0.12$, respectively) suggested to accept the null hypothesis and thus confirmed that the events in the air-filled pore space were randomly distributed. The sample-wise results are available in Table S2 (‘Root Epidermis excl. contact’) and Fig. S13.

The non-parametric estimates of the intensity as a function of the covariate (Fig. 4(a) - (d)) were in agreement with the aforementioned results: At small distances up to 0.05 mm, the estimated $\hat{\rho}(Z(u))$ were significantly below the estimated mean homogeneous intensity (red dashed line in Fig. 4) for all samples. At greater distances, the estimated functions oscillated around the mean value, but the deviations from a homogeneous intensity appeared non-significant.

The pooled Receiver Operating Characteristic (ROC) curve (Fig. 5(a)) and the corresponding area under the curve (AUC) reflected that the effect of the covariate ‘distance to soil particles’ on the intensity of the point process was weak. The ROC curves did not substantially deviate from the 1:1 line, meaning that the covariate had a low discriminatory power. This was confirmed by the mean AUC value of 0.57 ± 0.01 (Fig. 5(a)). The sample-wise ROC curves are presented in Fig. S16.

Inter-point dependence across the rhizosphere

To statistically evaluate hypothesis (2), stating that radially across the rhizosphere, root hairs were preferentially located in the close vicinity of soil particles, we repeated the spatial point pattern analysis at two specified distances from the root epidermis at (1) half and (2) the mean root hair length (rhizosphere cylinders 1 and 2). At distance (1), the analysis was based on a total of

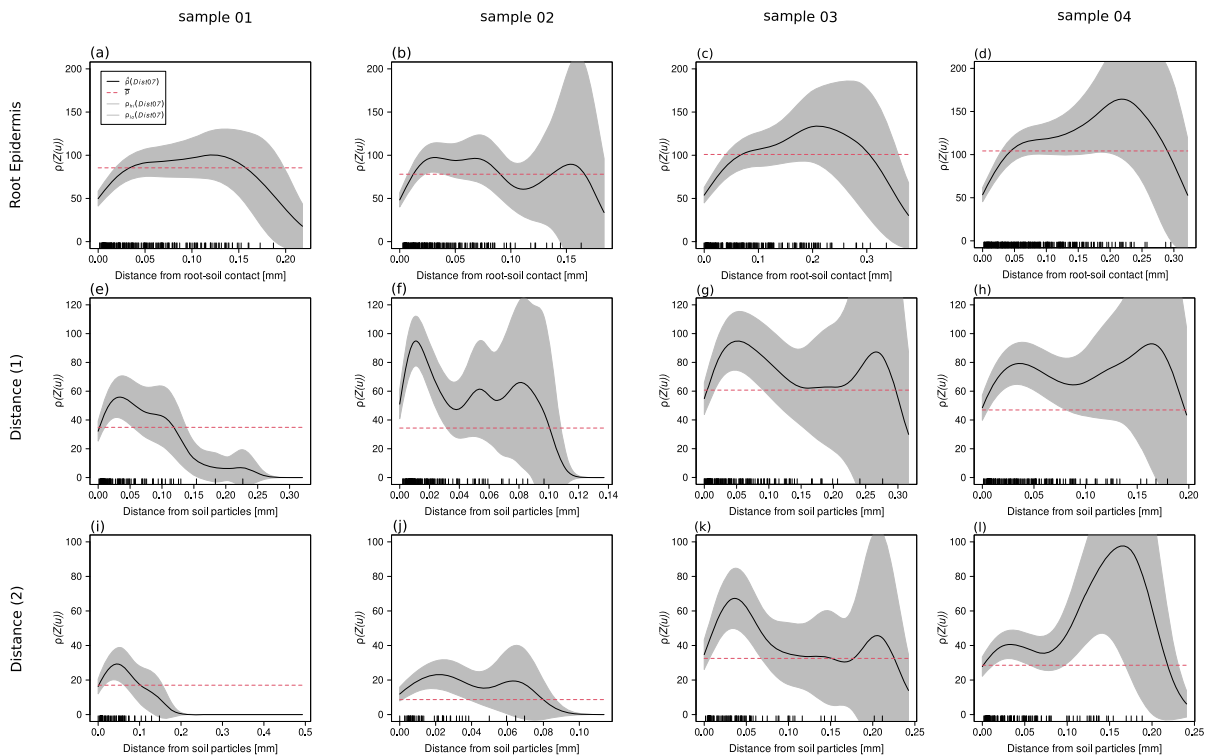


Fig. 4 Non-parametric estimation of the intensity of the point processes. Solid lines show the estimated functions, grey envelopes represent the 95% confidence band and the red dashed lines show the mean homogeneous intensities. (a) - (d): Estimated intensity of root hair emergence on the root epidermis as a function of the distance to soil particles. (e) - (h): Estimated

intensity of root hair intersection points at a radial distance of 122.75 μm from the root epidermis (rhizosphere cylinder 1) as a function of the distance to soil particles. (i) - (l): Estimated intensity of root hair intersection points at a radial distance of 245.5 μm from the root epidermis (rhizosphere cylinder 2) as a function of the distance to soil particles

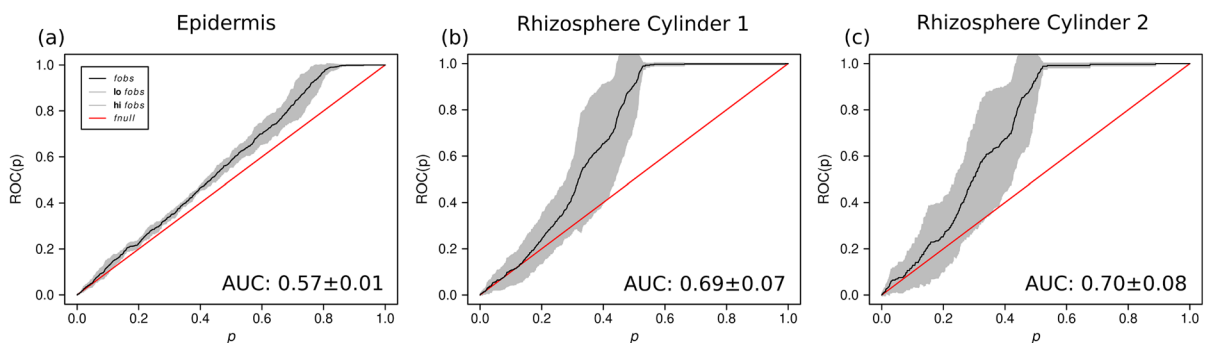


Fig. 5 Pooled receiver Operating Characteristic (ROC) curves. (a) ROC curves for root hair emergence points on the root epidermis. (b) ROC curves for root hair intersection points at a radial distance of 122.75 μm from the root epidermis (rhizosphere

cylinder 1). (c) ROC curves for root hair intersection points at a radial distance of 245.5 μm from the root epidermis (rhizosphere cylinder 2)

632 events at an intensity of $42.3 \pm 11.4 \text{ mm}^{-2}$, while at distance (2), the analysis was based on 368 events at an intensity of $20.9 \pm 9.2 \text{ mm}^{-2}$.

At both distances from the root epidermis, the pooled nearest neighbour distance distribution function ($G(r)$) (Fig. 2(c), (e)) deviated from CSR at inter-point distances $< 0.04 \text{ mm}$. On the other hand, the pooled empty space function ($F(r)$) did not systematically deviate from CSR. Nevertheless, except for the $G(r)$ -function of rhizosphere cylinder 2 (Fig. 2(e)) the pooled results of the DCLF-tests suggested to reject the null hypotheses stating that all studied patterns were CSR. Again, these deviations from CSR justified to further study the effect of the covariate ‘distance to soil particles’ on the distribution of events across the rhizosphere. The sample-wise results of the G- and F functions are presented in Fig. S6 - S8.

Inhomogeneous intensity of root hair distribution across the rhizosphere

The intensities of events at both radial distances from the root epidermis reflected the following trend: The intensity in tile one (rhizosphere cylinder-soil contact) was significantly smaller than the intensity in tile two (pore space close to soil particles; Fig. 6). The p-values

of the pooled chi-square tests at distance 1 and distance 2 were significant ($p < 2.2 \cdot 10^{-16}$ in both cases). The intensities in tile two were also larger than in tile three (pore space distant from soil particles). The chi-square tests were significant at both distances from the root epidermis ($p = 9.0 \cdot 10^{-4}$ and $p < 2.9 \cdot 10^{-5}$, respectively). In summary, the results suggested to reject the null hypothesis of homogeneity. They also indicated that the intensity of events radially across the rhizosphere was reduced at soil particles. It appears that root hairs rarely penetrated into soil aggregates. But the intensity was increased in the pore space close to soil particles and levelled again off at larger distances from the soil particles. The corresponding sample-wise results are presented in Fig. S10 and S11.

Similar results were found using the pooled Kolmogorov-Smirnov test. The results for the rhizosphere cylinders 1 and 2 were significant ($p < 2.2 \cdot 10^{-16}$ in both cases), suggesting to reject the null hypothesis of CSR. The sample-wise results of the Kolmogorov-Smirnov tests are available in Fig. S14 and S15.

The pooled Berman's Z2 tests were significant as well ($p < 2.2 \cdot 10^{-16}$ in both cases). The non-parametric estimates of the intensity (Fig. 4(e) - (l)) were in agreement with the quadrat counts: For both rhizosphere cylinders, the estimates $\hat{\rho}(Z(u))$ were

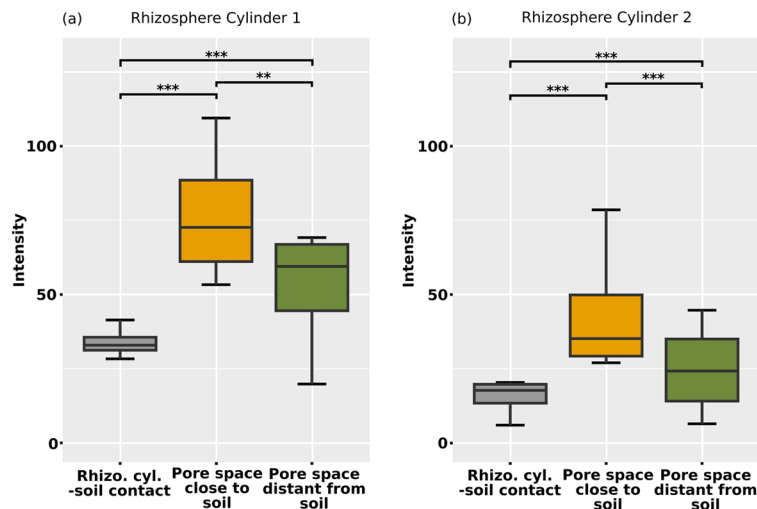


Fig. 6 Quadrat counting results for testing the dependence of the root hair intersection points on the covariate ‘distance to soil particles’. The intensity of events [$1/\text{mm}^2$] is plotted for the three tiles: rhizosphere cylinder - soil contact, pore space close to soil particles, and pore space distant from soil particles. (a) Results

for rhizosphere cylinder 1 (at a radial distance of $122.75 \mu\text{m}$ from the root epidermis). (b) Results for rhizosphere cylinder 2 (at a radial distance of $245.5 \mu\text{m}$ from the root epidermis). Significance levels taking the Bonferroni correction into account (*: $p < 0.017$, **: $p < 3.33 \cdot 10^{-4}$, ***: $p < 3.33 \cdot 10^{-4}$)

significantly above the estimated mean homogeneous intensity for small distances to soil particles (< 0.08 mm). At larger distances however, the estimates were significantly below the mean and converged against zero (Fig. 4(e), (f), (i), (j), (l)) or $\hat{\rho}$ did not differ significantly from CSR (Fig. 4(g), (h), (k)).

In summary, our results indicated that the intensities of the root hair intersection points on both rhizosphere cylinders depended on the spatial covariate ‘distance to soil particles’.

The pooled ROC curves (Fig. 5(b) and (c)) and the corresponding AUC values reinforced these results. The ROC curves deviated considerably from the 1:1 lines and the mean AUC were equal to 0.69 ± 0.07 and 0.7 ± 0.08 for rhizosphere cylinder 1 and 2, respectively.

Discussion

We found spatial patterning of root hairs in non-destructive *in situ* measurements of soil grown roots. Our results confirmed that root hairs emerged preferentially into air-filled macropores, while their emergence into partially water-saturated soil aggregates was inhibited. Furthermore, our results suggest that hairs emerged randomly into air-filled macropores, which explains the low discriminatory power of the covariate ‘distance to soil particles’ estimated based on the ROC-curve (Fig. 5(a)).

In addition, we found that at two specific radial distances from the root epidermis, root hairs were preferentially located in the pore space close to soil particles. In contrast, they were less abundant in the pore space distant from soil particles, and their occurrence was strongly inhibited within soil aggregates. However, our approach does not allow us to disentangle whether root hairs actually grew towards soil particles or whether they were pushed there by the moving menisci at the liquid–gas interface during the drying and rewetting cycles of the soil.

Our results suggest that root hairs bridge air-filled low-conductivity pores at the root-soil interface and establish contact with soil particles some radial distance away from the root-soil interface. While this mechanism attenuates the gradients in nutrient availability and water potential across the rhizosphere, their inability (in maize) to penetrate soil aggregates may limit root hair - soil contact and hence uptake

processes, plant anchorage, rhizosheath formation and root-microorganism interactions.

Based on these findings, we accept hypothesis (1a) stating that root hairs emerge preferentially into air-filled pore space. However, our results do not confirm hypothesis (1b) saying that root hairs emerge in the close vicinity of root-soil contact surfaces. Our results rather suggest that hairs emerge randomly into air-filled pores. Furthermore, we accept hypothesis 2, stating that radially across the rhizosphere, distal segments of root hairs are preferentially located in the vicinity of soil aggregates.

Root epidermal patterning

In contrast to other known root epidermal patterns (type II, e.g. in rice and type III, e.g. in *Arabidopsis*, Clowes 2000, Dolan 1996), in maize all root-epidermal cells can potentially generate a root hair. Thus, those cells that form root hairs (trichoblasts) are expected to be randomly distributed throughout the root epidermis (type I pattern, Hochholdinger et al. 2018, Salazar-Henao et al. 2016), and they are expected to be particularly plastic in response to environmental signals (Belimov et al. 2022, Cormack 1944, Hochholdinger et al. 2018). However, independent of the root epidermal pattern type, Bao et al. 2014 found that root hairs emerged at the air- rather than at the agar contact-side of their experimental setup. Regarding the patterning of lateral roots, the authors speculated that the water availability (as a product of soil hydraulic conductivity and soil water potential) may be the critical environmental signal. This may also apply for root hair patterning, but further investigation is needed to improve our understanding of this process.

While these findings were based on studies in artificial growth media (agar), White and Kirkegaard (2010) obtained similar results under physiologically relevant conditions. They surveyed in a microscopic analysis of soil cores containing a structured soil the abundance of wheat root hairs in cracks and pores. In agreement with Bao et al. (2014), they found a negative correlation between root-soil contact and root hair density. Our results are consistent with those reported by Bao et al. (2014) and White and Kirkegaard (2010). Unlike the study by White and Kirkegaard (2010), our experimental approach was non-destructive, but it was based on a sieved soil instead of field samples. Additionally,

the synchrotron-based X-ray μ CT approach allowed us to detect root hairs in the soil matrix.

Our finding that root hairs in maize hardly penetrated soil aggregates across the rhizosphere contradict the results presented by Koebernick et al. (2017). Using the same experimental approach as in our study (synchrotron-based X-ray μ CT), the authors showed that root hairs in barley disappeared on one side of soil aggregates but reappeared on another. This was explained by root hairs growing through soil aggregates. In maize, the latter was hardly observed and the discrepancy between these two species may be explained by differences in the ability of root hairs to overcome the mechanical resistance of the soil aggregates: The turgor pressure within the vacuole of maize root hairs may be lower than in barley. This would result in a lower maximum penetration force in maize.

Limitations

Studying inter-point dependence of root hair emergence on the epidermis, we found that inhibition occurred at small distances (< 0.06 mm). This could be explained by the fact that we determined the position of each root hair cell as a point with infinitesimal extent. We thereby neglected the spatial extent of the root hair cells. Hence, there was a physical boundary as to how close events could get to each other. We assumed in our analysis that we determined the centres of the hairs, but we are aware that the manual segmentation of root hair emergence points introduced some errors. We accounted for this by assuming that at the root epidermis, root hairs were in contact with soil particles at distances up to the diameter of root hair cells (0.0215 mm). At the two rhizosphere cylinders, we assumed that the minimum distance between soil particles and root hairs was equal to the mean diameter of root hairs (0.01788 mm). By considering the diameters of hair cells and hairs rather than the corresponding radii, we chose conservative estimates. Although the characteristic interaction between events is considered in the Gibbs hard core process (Baddeley et al. 2015, Illian et al. 2008, Wiegand and Moloney 2013), we based our analysis on the assumption of a Poisson process. This was justified by the fact that the spatial extents of the observation windows were about two orders of magnitude larger than the root hair radii.

Furthermore, our approach neglected the anisotropy of epidermal cells. Their length is considerably larger than their diameter: As reported by Zidan et al. (1990) and Moreno-Ortega et al. (2017), they reach lengths of up to 0.2 mm.

It is worth noting that the replicated point pattern analysis is based on the assumptions that the four samples are comparable to each other and that they are independent replications of the same point process. Further limitations of our approach relate to the segmentation of root hairs. While their classification within air-filled pores was straightforward, we are aware that their segmentation within soil aggregates is more prone to errors. This is due to the lower contrast between partially saturated soil aggregates and root hairs. Therefore, under-segmentation of root hairs (especially within soil aggregates) cannot be excluded.

Another limitation is related to the unwrapping procedure that was applied prior to the spatial point pattern analysis. We unwrapped the epidermis of the root segments under the assumption of cylindrical roots of constant radii and we are aware that this simplification may have introduced errors.

Additionally, the growth conditions within the experimental setup are likely to have introduced limitations. Clearly the environmental conditions within our experimental setup were not comparable to field conditions due to the limited size of the plastic cylinders and the fact that we used a sieved soil. However, the microcosms were required in order to collect high-resolution μ CT data. The increased soil porosity along the plastic cylinder walls may have created favourable root growth paths. We corrected for this effect by excluding parts of the root epidermis where there were no soil particles between the cylinder wall and the root, or where roots were even in contact with the cylinder wall.

Implications and outlook

Our findings contribute to the ongoing discussion on root plasticity as breeding target for more productive crops (Schneider and Lynch 2020). The authors emphasised that in low input environments, plastic root phenotypes are beneficial for exploiting inhomogeneously distributed soil resources. The fact that root hairs preferentially emerged into air-filled pore space and not into soil aggregates suggests that they bridge air-filled (low conductivity) gaps at the root-soil interface. Thereby,

they attenuate gradients in nutrient availability and water potential throughout the rhizosphere (Duddek et al. 2023, Keyes et al. 2013). Nevertheless, as they rarely grew through soil aggregates (in maize), their contact with soil particles is expected to be markedly reduced compared to hairs growing randomly through the rhizosphere (and thus penetrating into soil aggregates). This may be part of the explanation of discrepancies in the effect of root hairs on root water uptake observed for different crop species such as barley and maize (Cai et al. 2021, Carminati et al. 2017). It is also expected to affect both plant anchorage and rhizosheath formation. Root hairs growing through soil aggregates are hypothesized to experience a greater adhesion to soil particles, which may increase uprooting resistance and the rhizosheath thickness.

Our results have implications for mathematical modelling of nutrient and water uptake, too. The spatial distribution of root hairs relative to soil particles is of particular interest under dry soil conditions, when macropores are drained and both nutrient and water transport are limited to the soil micropore region. So far, the spatial distribution of root hairs in relation to soil particles is inherently included in image-based models (Daly et al. 2016, Duddek et al. 2023, Keyes et al. 2013). However, these models are computationally highly demanding and homogenized (multi-scale) models are needed to predict root resource acquisition at bigger scales. Up-scaled models are usually based on the assumption of uniformly distributed hairs in a homogeneous soil domain (Itoh and Barber 1983, Leitner et al. 2010, Segal et al. 2008, Zygalkakis et al. 2011). However, our results suggest that this leads to an oversimplification of the rhizosphere, neglecting in particular the plasticity of roots and root hairs to environmental triggers on the one hand, and distinct hydraulic parameters of the rhizosphere compared to the bulk soil on the other. Depending on the model assumptions, this masks the rhizosphere and especially the root hair effect. Therefore, our analysis has the potential to improve the generation of up-scaled root models with respect to a variety of plant-relevant processes.

Acknowledgements This project was carried out in the framework of the priority program 2089 “Rhizosphere spatiotemporal organization - a key to rhizosphere functions” funded by DFG, German Research Foundation (project number 403670197). We thank Caroline Marcon and Frank Hochholding (University of Bonn) for providing the maize B73 seeds. We also thank Patrick von Jeetze (Potsdam Institute for Climate Impact), Luise

Ohmann (Helmholtz Centre for Environmental Research (UFZ) Halle) and Nicolai Koebernick (Root-Soil Interaction, Technical University Munich) for assistance with data collection. We acknowledge the Paul Scherrer Institute, Villigen, Switzerland for provision of synchrotron radiation beamtime at the TOMCAT beamline X02DA of the SLS. Open access funding was provided by ETH Zürich.

Author contributions M.A.A and A.C. conceived and designed the experiments for the TOMCAT beamline (PSI, Switzerland). M.A.A. performed the measurements at the TOMCAT beamline (PSI, Switzerland). P.D. processed and segmented the image data. P.D. A.P. and A.C. conceived and designed the statistical analysis of the data. P.D. and A.P. performed the statistical analysis with contributions from A.C. P.D. wrote the manuscript with contributions from A.P. and A.C. G.L. provided technical assistance as a beamline scientists at the TOMCAT beamline (PSI, Switzerland). All authors contributed to editing and revising the manuscript.

Funding Information Open access funding provided by Swiss Federal Institute of Technology Zurich.

Data Availability Statement The data supporting the results of this study are available in the ETH Zürich Research Collection (doi: 10.3929/ethz-b-000670450 and 10.3929/ethz-b-000619872) and can be accessed via the following links: <http://hdl.handle.net/20.500.11850/670450> and <http://hdl.handle.net/20.500.11850/619872>.

Declarations

Competing Interests None declared.

Open Access This article is licensed under a Creative Commons Attribution 4.0 International License, which permits use, sharing, adaptation, distribution and reproduction in any medium or format, as long as you give appropriate credit to the original author(s) and the source, provide a link to the Creative Commons licence, and indicate if changes were made. The images or other third party material in this article are included in the article's Creative Commons licence, unless indicated otherwise in a credit line to the material. If material is not included in the article's Creative Commons licence and your intended use is not permitted by statutory regulation or exceeds the permitted use, you will need to obtain permission directly from the copyright holder. To view a copy of this licence, visit <http://creativecommons.org/licenses/by/4.0/>.

References

- Anderson EL, Millner PD, Kunishi HM (1987) Maize root length density and mycorrhizal infection as influenced by tillage and soil phosphorus. *J Plant Nutr* 10(9–16):1349–1356. <https://doi.org/10.1080/01904168709363667>
- Baddeley A, Gill RD (1997) Kaplan-Meier estimators of distance distributions for spatial point processes. *Ann Stat* 25(1):263–292. <https://doi.org/10.1214/aos/1034276629>

- Baddeley A, Chang Y-M, Song Y, Turner R (2012) Nonparametric estimation of the dependence of a spatial point process on spatial covariates. *Stat Interface* 5(2):221–236. <https://doi.org/10.4310/SII.2012.v5.n2.a7>
- Baddeley A, Rubak E, Turner R (2015) *Spatial Point Patterns: Methodology and Applications with R*. CRC Press. Google Books: rGbmCgAAQBAJ
- Bao Y, Aggarwal P, Robbins NE, Sturrock CJ, Thompson MC, Tan HQ, Dinneny JR (2014) Plant roots use a patterning mechanism to position lateral root branches toward available water. *Proc Natl Acad Sci* 111(25):9319–9324. <https://doi.org/10.1073/pnas.1400966111>
- Bates TR, Lynch JP (1996) Stimulation of root hair elongation in *Arabidopsis thaliana* by low phosphorus availability. *Plant Cell Environ* 19(5):529–538. <https://doi.org/10.1111/j.1365-3040.1996.tb00386.x>
- Belimov A, Ulianich P, Syrova D, Shaposhnikov A, Safronova V, Dodd I (2022) Modulation of tomato root architecture and root hair traits by *Pseudomonas brassicacearum* and *Variovorax paradoxus* containing 1-aminocyclopropane-1-carboxylate deaminase. *Biologia Plantarum* 66:228–239. <https://doi.org/10.32615/bp.2022.025>
- Bengough AG, Loades K, McKenzie BM (2016) Root hairs aid soil penetration by anchoring the root surface to pore walls. *J Exp Bot* 67(4):1071–1078. <https://doi.org/10.1093/jxb/erv560.pmid:26798027>
- Ben-Said M (2021) Spatial point-pattern analysis as a powerful tool in identifying pattern-process relationships in plant ecology: An updated review. *Ecol Process* 10(1):56. <https://doi.org/10.1186/s13717-021-00314-4>
- Berman M (1986) Testing for Spatial Association Between a Point Process and An727 other Stochastic Process. *J R Stat Soc Ser C (Appl Stat)* 35(1):54–62. <https://doi.org/10.2307/2347865.JSTOR:2347865>
- Bibikova T, Gilroy S (2002) Root Hair Development. *J Plant Growth Regul* 21(4):383–415. <https://doi.org/10.1007/s00344-003-0007-x>
- Blender Online Community (2022) Blender - a 3D modelling and rendering package (Version 3.0.1). <http://www.blender.org>
- Bünning E (1951) Über die Differenzierungsvorgänge in der Cruciferenwurzel. *Planta* 39(2):126–153. <https://doi.org/10.1007/BF01910114>
- Burak E, Quinton JN, Dodd IC (2021) Root hairs are the most important root trait for rhizosphere formation of barley (*Hordeum vulgare*), maize (*Zea mays*) and *Lotus japonicus* (Gifu). *Ann Bot* 128(1):45–57. <https://doi.org/10.1093/aob/mcab029>
- Cai G, Carminati A, Abdalla M, Ahmed MA (2021) Soil textures rather than root hairs dominate water uptake and soil-plant hydraulics under drought. *Plant Physiol* 187(2):858–872. <https://doi.org/10.1093/plphys/kiab271>
- Carminati A, Moradi AB, Vetterlein D, Vontobel P, Lehmann E, Weller U, Oswald SE (2010) Dynamics of soil water content in the rhizosphere. *Plant and Soil* 332(1):163–176. <https://doi.org/10.1007/s11104-010-0283-8>
- Carminati A, Passioura JB, Zarebanadkouki M, Ahmed MA, Ryan PR, Watt M, Delhaize E (2017) Root hairs enable high transpiration rates in drying soils. *New Phytol*, 216(3):771–781. JSTOR: 90015071. Retrieved November 21, 2022, <https://www.jstor.org/stable/90015071>
- Clowes Fal (2000) Pattern in root meristem development in angiosperms. *New Phytol* 146(1):83–94. <https://doi.org/10.1046/j.1469-8137.2000.00614.x>
- Cormack RGH (1944) The Effect of Environmental Factors on the Development of Root Hairs in *Phleum pratense* and *Sporobolus cryptandrus*. *Am J Bot* 31(7):443–449. <https://doi.org/10.2307/2437304.JSTOR:2437304>
- Cormack RGH (1947) A Comparative Study of Developing Epidermal Cells in White Mustard and Tomato Roots. *Am J Bot* 34(6):310–314. <https://doi.org/10.1002/j.1537-2197.1947.tb12994.x>
- Daly KR, Keyes SD, Masum S, Roose T (2016) Image-based modelling of nutrient movement in and around the rhizosphere. *J Exp Bot* 67(4):1059–1070. <https://doi.org/10.1093/jxb/erv544>
- Diggle P (2013) *Statistical analysis of spatial and spatio-temporal point patterns*. CRC Press. <https://books.google.ch/books?id=5FHSBQAAQBAJ>
- Dolan L, Duckett CM, Grierson C, Linstedt P, Schneider K, Lawson E, Roberts K (1994) Clonal relationships and cell patterning in the root epidermis of *Arabidopsis*. *Development* 120(9):2465–2474. <https://doi.org/10.1242/dev.120.9.2465>
- Dolan L (1996) Pattern in the Root Epidermis: An Interplay of Diffusible Signals and Cellular Geometry. *Ann Bot* 77(6):547–553. <https://doi.org/10.1006/anbo.1996.0069>
- Dolan L, Costa S (2001) Evolution and genetics of root hair stripes in the root epidermis. *J Exp Bot* 52:413–417. https://doi.org/10.1093/jexbot/52.suppl_1.413
- Duddek P, Carminati A, Koebernick N, Ohmann L, Lovric G, Delzon S, Ahmed MA (2022) The impact of drought-induced root and root hair shrinkage on root-soil contact. *Plant Physiol* 189(3):1232–1236. <https://doi.org/10.1093/plphys/kiac144>
- Duddek P, Ahmed MA, Javaux M, Vanderborght J, Lovric G, King A, Carminati A (2023) The effect of root hairs on root water uptake is determined by root-soil contact and root hair shrinkage. *New Phytol*, n/a(n/a). <https://doi.org/10.1111/nph.19144>
- Foehse D, Jungk A (1983) Influence of phosphate and nitrate supply on root hair formation of rape, spinach and tomato plants. *Plant and Soil* 74(3):359–368. <https://doi.org/10.1007/BF02181353>
- Giehl RFH, von Wirén N (2018) Hydropatterning-how roots test the waters. *Science* 362(6421):1358–1359. <https://doi.org/10.1126/science.aav9375>
- Girardeau-Montaut D (2022) CloudCompare - Documentation (Version 2.12). Retrieved July 17, 2023, <https://www.cloudcompare.org/doc/>
- Gregory P (2006) Roots, rhizosphere and soil: The route to a better understanding of soil science? *Eur J Soil Sci* 57(1):2–12. <https://doi.org/10.1111/j.1365-2389.2005.00778.x>
- Haling RE, Brown LK, Bengough AG, Young IM, Hallett PD, White PJ, George TS (2013) Root hairs improve root penetration, root-soil contact, and phosphorus acquisition in soils of different strength. *J Exp Bot* 64(12):3711–3721. <https://doi.org/10.1093/jxb/ert200>
- Hinsinger P, Bengough AG, Vetterlein D, Young IM (2009) Rhizosphere: Biophysics, biogeochemistry and ecological relevance. *Plant and Soil* 321(1):117–152. <https://doi.org/10.1007/s11104-008-9885-9>

- Hochholdinger F, Yu P, Marcon C (2018) Genetic Control of Root System Development in Maize. *Trends Plant Sci* 23(1):79–88. <https://doi.org/10.1016/j.tplants.2017.10.004>
- Holz M, Zarebanadkouki M, Kuzyakov Y, Pausch J, Carminati A (2018) Root hairs increase rhizosphere extension and carbon input to soil. *Ann Bot* 121(1):61–69. <https://doi.org/10.1093/aob/mcx127>
- Illian J, Penttinen A, Stoyan H, Stoyan D (2008) *Statistical Analysis and Modelling of Spatial Point Patterns* (1 ed). Chichester, England ; Hoboken, NJ: Wiley-Interscience
- Itoh S, Barber SA (1983) A numerical solution of whole plant nutrient uptake for soil-root systems with root hairs. *Plant and Soil* 70(3):403–413. <https://doi.org/10.1007/BF02374895>
- Keyes SD, Daly KR, Gostling NJ, Jones DL, Talboys P, Pinzer BR, Roose T (2013) High resolution synchrotron imaging of wheat root hairs growing in soil and image based modelling of phosphate uptake. *New Phytol* 198(4):1023–1029. <https://doi.org/10.1111/nph.12294>
- Koebnick N, Daly KR, Keyes SD, George TS, Brown LK, Raffan A, Roose T (2017) High-resolution synchrotron imaging shows that root hairs influence rhizosphere soil structure formation. *New Phytol* 216(1):124–135. <https://doi.org/10.1111/nph.14705>
- Kolmogorov A (1933) Sulla determinazione empirica di una legge di distribuzione. *G. Ist. Ital. Attuari*, 4, 83–91. Retrieved July 18, 2023, <https://cir.nii.ac.jp/crid/1571135650766370304>
- Lavelle P (2002) Functional domains in soils. *Ecol Res* 17(4):441–450. <https://doi.org/10.1046/j.1440-1703.2002.00509.x>
- Leitner D, Klepsch S, Ptashnyk M, Marchant A, Kirk GJD, Schnepf A, Roose T (2010) A dynamic model of nutrient uptake by root hairs. *New Phytol* 185(3):792–802. <https://doi.org/10.1111/j.1469-8137.2009.03128.x>
- Ma Z, Bielenberg DG, Brown KM, Lynch JP (2001) Regulation of root hair density by phosphorus availability in *Arabidopsis thaliana*. *Plant Cell Environ* 24(4):459–467. <https://doi.org/10.1046/j.1365-3040.2001.00695.x>
- Mackay AD, Barber SA (1985) Effect of soil moisture and phosphate level on root hair growth of corn roots. *Plant and Soil* 86(3):321–331. <https://doi.org/10.1007/BF02145453>
- Mackay AD, Barber SA (1987) Effect of cyclic wetting and drying of a soil on root hair growth of maize roots. *Plant and Soil* 104(2):291–293. <https://doi.org/10.1007/BF02372544>
- Marin M, Feeney DS, Brown LK, Naveed M, Ruiz S, Koebnick N, George TS (2021) Significance of root hairs for plant performance under contrasting field conditions and water deficit. *Ann Bot* 128(1):1–16. <https://doi.org/10.1093/aob/mcaa181>
- Miguel MA, Postma JA, Lynch JP (2015) Phene Synergism between Root Hair Length and Basal Root Growth Angle for Phosphorus Acquisition. *Plant Physiol* 167(4):1430–1439. <https://doi.org/10.1104/pp.15.00145>
- Misra RK, Alston AM, Dexter AR (1988) Role of root hairs in phosphorus depletion from a macrostructured soil. *Plant and Soil* 107(1):11–18. <https://doi.org/10.1007/BF02371538>
- Moreno-Ortega, B., Fort, G., Muller, B., Guédon, Y. (2017). Identifying Developmental Zones in Maize Lateral Root Cell Length Profiles using Multiple Change-Point Models. *Frontiers in Plant Science*, 8. Retrieved January 15, 2024, <https://www.frontiersin.org/articles/10.3389/fpls.2017.01750>
- Müller M, Schmidt W (2004) Environmentally Induced Plasticity of Root Hair Development in *Arabidopsis*. *Plant Physiol* 134(1):409–419. <https://doi.org/10.1104/pp.103.029066.pmid:14730071>
- Neyman J, Pearson ES (1928) On the Use and Interpretation of Certain Test Criteria for Purposes of Statistical Inference: Part I. *Biometrika* 20A(1/2):175–240. <https://doi.org/10.2307/2331945.JSTOR:2331945>
- Orosa-Puente B, Leftley N, von Wangenheim D, Banda J, Srivastava AK, Hill K, Bennett MJ (2018) Root branching toward water involves posttranslational modification of transcription factor ARF7. *Science* 362(6421):1407–1410. <https://doi.org/10.1126/science.aau3956>
- Pemberton LMS, Tsai S-L, Lovell PH, Harris PJ (2001) Epidermal Patterning in Seedling Roots of Eudicotyledons. *Ann Bot* 87(5):649–654. <https://doi.org/10.1006/anbo.2001.1385>
- RCore Team (2022) R: A language and environment for statistical computing. manual. Vienna, Austria: R Foundation for Statistical Computing. <https://www.R-project.org/>
- Robbins NE, Dinneny JR (2015) The divining root: Moisture-driven responses of roots at the micro- and macro-scale. *J Exp Bot* 66(8):2145–2154. <https://doi.org/10.1093/jxb/eru496.pmid:25617469>
- Rodríguez-Álvarez MX, Boer MP, van Eeuwijk FA, Eilers PH (2017) Correcting for spatial heterogeneity in plant breeding experiments with P-splines. *Spat Stat* 23:52–71. <https://doi.org/10.1016/j.spasta.2017.10.003>
- RStudio Team (2022) RStudio: Integrated Development Environment for R (Version 2022.02.3). Boston, MA. <http://www.rstudio.com/>
- Salazar-Henao JE, Vélez-Bermúdez IC, Schmidt W (2016) The regulation and plasticity of root hair patterning and morphogenesis. *Development* 143(11):1848–1858. <https://doi.org/10.1242/dev.132845>
- Schneider HM, Lynch JP (2020) Should Root Plasticity Be a Crop Breeding Target? *Frontiers in Plant Science*, 11. Retrieved July 10, 2023, <https://www.frontiersin.org/articles/10.3389/fpls.2020.00546>
- Segal E, Kushnir T, Mualem Y, Shani U (2008) Water Uptake and Hydraulics of the Root Hair Rhizosphere. *Vadose Zone J* 7(3):1027–1034. <https://doi.org/10.2136/vzj2007.0122>
- Singh Gahoonia T, Care D, Nielsen NE (1997) Root hairs and phosphorus acquisition of wheat and barley cultivars. *Plant and Soil* 191(2):181–188. <https://doi.org/10.1023/A:1004270201418>
- Stuedle E, Oren R, Schulze E-D (1987) Water Transport in Maize Roots: Measurement of Hydraulic Conductivity, Solute Permeability, and of Reflection Coefficients of Excised Roots Using the Root Pressure Probe. *Plant Physiology* 84(4):1220–1232. <https://doi.org/10.1104/pp.84.4.1220>
- Thermo Fisher Scientific (2020) Avizo Software for Materials Research: Materials Characterization and Quality Control (Version 2020.1). <https://assets.thermofisher.com/TFS-Assets/MSD/brochures/brochure-avizo-software-materials887research.pdf>
- Vetterlein D, Lippold E, Schreiter S, Phalempin M, Fahrenkamp T, Hochholdinger F, Schlüter F (2021) Experimental platforms for the investigation of spatiotemporal patterns in the

- rhizosphere-Laboratory and field scale. *J Plant Nutr Soil Sci* 184(1):35–50. <https://doi.org/10.1002/jpln.202000079>
- Watt M, Silk WK, Passioura JB (2006) Rates of root and organism growth, soil conditions, and temporal and spatial development of the rhizosphere. *Ann Bot* 97(5):839–855. <https://doi.org/10.1093/aob/mcl028>
- White RG, Kirkegaard JA (2010) The distribution and abundance of wheat roots in a dense, structured subsoil - implications for water uptake. *Plant Cell Environ* 33(2):133–148. <https://doi.org/10.1111/j.1365-3040.2009.02059.x>
- Wiegand T, Moloney KA (2013) *Handbook of Spatial Point-Pattern Analysis in Ecology* (1st ed). Boca Raton: Taylor & Francis Ltd
- Wilson DJ (2019) The harmonic mean p-value for combining dependent tests. *Proc Natl Acad Sci U S A* 116(4):1195–1200 <https://www.pnas.org/content/116/4/1195>
- Zhang Y, Yang Z, Zhang Z, Li Y, Guo J, Liu L, Han G (2023) Root Hair Development and Adaptation to Abiotic Stress. *J Agric Food Chem*. <https://doi.org/10.1021/acs.jafc.2c07741>
- Zhu J, Kaeppler SM, Lynch JP (2005) Mapping of QTL controlling root hair length in maize (*Zea mays* L.) under phosphorus deficiency. *Plant and Soil* 270(1):299–310. <https://doi.org/10.1007/s11104-004-1697-y>
- Zhu J, Zhang C, Lynch JP (2010) The utility of phenotypic plasticity of root hair length for phosphorus acquisition. *Funct Plant Biol* 37(4):313–322. <https://doi.org/10.1071/FP09197>
- Zidan I, Azaizeh H, Neumann PM (1990) Does Salinity Reduce Growth in Maize Root Epidermal Cells by Inhibiting Their Capacity for Cell Wall Acidification? 1. *Plant Physiol* 93(1):7–11. <https://doi.org/10.1104/pp.93.1.7>
- Zygalakis KC, Kirk GJD, Jones DL, Wissuwa M, Roose T (2011) A dual porosity model of nutrient uptake by root hairs. *New Phytol* 192(3):676–688. <https://doi.org/10.1111/j.1469-8137.2011.03840.x>

Publisher's Note Springer Nature remains neutral with regard to jurisdictional claims in published maps and institutional affiliations.